

FOCUSING ON THE FIXED POINT OF 4D SIMPLICIAL GRAVITY

P. Bialas^{a1}, Z. Burda^{b2}, A. Krzywicki^c and B. Petersson^{b3}

^a Inst. Theor. Fysica, Universiteit van Amsterdam, 1018 XE Amsterdam,
The Netherlands

^b Fakultät für Physik, Universität Bielefeld, Postfach 10 01 31, D-33501
Bielefeld, Germany

^c Laboratoire de Physique Théorique et Hautes Energies, Bât. 211,
Université de Paris-Sud, 91405 Orsay, France⁴

Abstract

Our earlier renormalization group analysis of simplicial gravity is extended. A high statistics study of the volume and coupling constant dependence of the cumulants of the node distribution is carried out. It appears that the phase transition of the theory is of first order, contrary to what is generally believed .

January 1996
LPTHE Orsay 96/08
BI-TP 96/05
ITFA-96-2

¹Permanent address: Inst. Comp. Science, Jagellonian University, ul. Nawojki 11, 30-072 Kraków, Poland.

²Permanent adress: Inst. of Physics, Jagellonian University, ul. Reymonta 4, 30-059 Kraków, Poland.

³bengt@phyaserv.uni-bielefeld.de

⁴Laboratoire associé au CNRS.

1. Introduction

The aim of this paper is to present results obtained in a numerical study of the critical behavior of simplicial gravity in four dimensions ($4d$). We limit our attention to manifolds with the topology of a sphere, discretized according to the dynamical triangulation recipe [1]. The paper has two facets: we extend our recent investigation [2] of volume-volume correlations using the renormalization group (RG) techniques and we examine the finite-size scaling of the integrals of 2- and 3-point curvature-curvature correlation functions. We attempt to achieve a better understanding of the theory putting together the two sets of data.

A warning is in order before we proceed further. It is obvious that we move in an almost uncharted territory. Our guide are analogies with more conventional field theory and/or statistical mechanics and we are well aware of the fact that these analogies might be misleading. Therefore, we try to clearly separate the presentation of our data from the speculations.

The plan of the paper is the following: in sect. 2 we briefly describe the lattice gravity model studied here as well as the numerical algorithm employed in our computer simulations. Sect. 3 is devoted to the RG analysis. In sect. 4 the results concerning the node distribution are presented. These results indicate, to our surprise, that the phase transition is presumably of first order. The last section contains the discussion and conclusions. A summary of data is presented in tables grouped in the Appendix.

2. Model and numerical algorithm

The model is identical to that studied in [2]. Thus, we take an Euclidean version of the Einstein-Hilbert action, which for a $4d$ simplicial manifold reads

$$S = -\kappa_2 N_2 + \kappa_4 N_4 \tag{1}$$

Here N_k denotes the total number of k -simplexes. The theory is defined by the partition function

$$Z(\kappa_2, \kappa_4) = \sum_{N_2 N_4} Z_{N_2 N_4} e^{-S} \tag{2}$$

where

$$Z_{N_2 N_4} = \sum_{T(N_2, N_4)} W(T) \quad (3)$$

The summation is over fixed topology $4d$ simplicial manifolds $T(N_2, N_4)$ and $W(T)$ is the symmetry factor taking care of the equivalent relabelings of a manifold.

We are interested in a fixed N_4 canonical ensemble of spherical manifolds with the partition function:

$$Z(\kappa_2, N_4) = \sum_{N_2} Z_{N_2 N_4} e^{-S} \quad (4)$$

As in [2] we actually simulate a grand-canonical ensemble, but with a quadratic potential term $\frac{1}{2}\delta(N_4 - \bar{N}_4)^2$ added to the action so that the value of N_4 at which the measurements are done is highly probable in the resulting N_4 distribution. This is the standard procedure. The volume fluctuations hopefully insure the ergodicity of the updating algorithm (cf. [3]). In most of the work we used $\delta = 0.005$.

The algorithm used in this paper comprises the five standard local moves supplemented by the global “baby universe surgery” [4, 5]. The local moves are equiprobable. One local sweep is made up of N_4 attempts to perform a local move. “Baby universe surgery” consists in cutting out and gluing back, but at another place, minimum neck baby universes (minBUs). All minBU necks are identified but only minBUs with volume larger than some lower cut-off are actually moved (the cut-off is set for definiteness to 20 simplexes). After having identified all necks the “surgery” is attempted a number of times equal to twice the number of minBU necks. In a typical run nine sweeps of local moves are followed by one global sweep. The CPU time needed to perform a global sweep depends on the number of baby universes and therefore on κ_2 . In the neighbourhood of the critical point it is of the same order of magnitude as the time needed to perform a sweep of local moves.

The global moves reduce the autocorrelation times dramatically in the so-called cold phase, where the manifolds are highly branched. They help much less elsewhere. In the vicinity of the critical point minBU surgery reduces the autocorrelation time but does not prevent the critical slowing down to manifest itself vigorously. We show in Fig. 1 the time averaged integral of

the autocorrelation function, denoted by τ , for a set of values of κ_2 and N_4 . We have measured N_0 once every 10 sweeps ⁵ (local and global sweeps are counted on the same footing).

3. Monte Carlo Renormalization Group

We follow the approach proposed in [2] based on the hierarchical baby-universe structure of a typical dynamically triangulated manifold. The RG transformation, appropriately called *fractal blocking* in ref. [6], consists in cutting the outer layer of minBUs.

Let $|x_A - x_B|$ denote the geodesic distance between simplexes A and B (i.e. the minimum number of steps, along the dual lattice, separating A and B). The correlation function

$$G(r) = \langle N_4^{-2} \sum_{AB} \delta(r - |x_A - x_B|) \rangle \quad (5)$$

characterizes the global geometry of the manifold. Its moments $\langle r^k \rangle$, $k = 1, 2, \dots$, are dimensionless lattice observables which transform under RG as $\langle r_{in} \rangle \rightarrow \langle r_{out} \rangle = \langle r_{in} \rangle - \delta r$, etc.

Our RG transformation can be regarded as corresponding to the increase of the lattice spacing a . Indeed, let us keep fixed the physical volume $N_4 a^4$ of the manifold. Then

$$\delta \ln \frac{1}{a} = \frac{1}{4} \delta \ln N_4 \quad (6)$$

This change of the resolution should be accompanied by a shift of coupling constants. Assuming that κ_2 is the only coupling that matters for the global shape of the manifold one writes

$$\delta r = r_N \delta \ln N_4 + r_\kappa \delta \kappa_2 \quad (7)$$

where r_N and r_κ denote partial derivatives of $\langle r \rangle$ with respect to $\ln N_4$ and κ_2 . Eq. (7) is used to find $\delta \kappa_2$ and, together with (6) to estimate the β -function defined by

$$\beta(\kappa_2) = \frac{\partial \kappa_2}{\partial \ln \frac{1}{a}} \quad (8)$$

⁵We have checked that at the phase transition point the frequency of passes through $N_4 = \bar{N}_4$ is the same in both phases.

We have calculated the β -function for $N_4 = 4000, 8000$ and 16000 . The results are shown in Fig. 2.

Of course, one could use another moment of $G(r)$. If our philosophy is correct the resulting β -function should be the same as before, at least in the limit of very large N_4 . We have measured $\langle r^2 \rangle$ along with $\langle r \rangle$. The β -function obtained using $\sqrt{\langle r^2 \rangle}$ is almost undistinguishable from that calculated from $\langle r \rangle$.

We have also computed the ratio

$$B = \frac{\sqrt{\langle r_{in}^2 \rangle} / \langle r_{in} \rangle}{\sqrt{\langle r_{out}^2 \rangle} / \langle r_{out} \rangle}, \quad (9)$$

which is found to be very close to unity for all values of κ_2 and N_4 considered in this paper. The best fit to $B = \text{const}$ yields $1.0014(56)$, $0.9993(54)$ and $1.0009(31)$ for $N_4 = 4000, 8000$ and 16000 respectively. Thus, the shape of $G(r)$ is approximately constant along the RG flow provided that r is measured in units of $\langle r \rangle$ (compare with [7]).

These results are nicely self-consistent and confirm the results presented in [2]. The zero of the β -function is close to the position of the critical point determined by different methods. It moves up in κ_2 as N_4 increases but seems to converge to a limiting value.

The slope of the β -function does not vary significantly with N_4 . The average value obtained combining data at $N_4 = 4000, 8000$ and 16000 is $\beta_0 \equiv -\beta'(\kappa_2^*) = 7.32(46)$. This value should be for the moment taken with circumspection: we do not know how reliable is our blocking scheme. It would be interesting to calculate this parameter using another RG blocking scheme, for example one derived from the proposal set forth in Ref. [6].

As already explained in [2] our blocking operation cannot be iterated. This would require being able to cut baby universes with necks larger than the minimum one, which is very difficult to implement. Thus the standard method of estimating finite-size corrections, which consists in comparing results at the same lattice volume but after different number of blocking steps, cannot be applied here. All we can do is to compare data obtained at different volumes.

Consider now the intrinsic Hausdorff dimension d_H . It has been observed in refs. [5, 7, 8, 9] that d_H is very large, perhaps infinite, in the hot phase

and close to 2 in the cold one. Indeed (and this can be also seen in the tables presented in the Appendix) $\langle r \rangle$ depends weakly on N_4 below the critical point and rises roughly like $N_4^{1/2}$ above it. This result concerns d_H computed at *fixed* κ_2 . However, as already mentioned in [2], it is rather the value of d_H attached to a RG trajectory which has a real physical significance. Unfortunately, our calculation of the β -function does not extend to large enough lattices and is not sufficiently precise to make possible a serious determination of RG trajectories. We can, however, use the obvious equation

$$d_H = \langle r \rangle \delta \ln N_4 / \delta r \quad (10)$$

to estimate the (effective) fractal dimension locally, on a RG trajectory passing through a given point in the (N_4, κ_2) plane. Points close to κ_2^* are of particular interest. Using the RG data given in the Appendix we find at $N_4 = 8000$ the fractal dimensions 3.7(1.4) and 4.4(1.3) for $\kappa_2 = 1.200$ and 1.225, respectively. At $N_4 = 16000$ we obtain $d_H = 4.0(1.4), 5.3(2.6)$ and $5.7(2.9)$ for $\kappa_2 = 1.225, 1.238$ and 1.250 , respectively (see [7] for a similar result).

4. Finite-size scaling analysis

Our next set of data concerns the (normalized) cumulants of the distribution of the number N_0 of nodes of the lattice:

$$\begin{aligned} c_2(N_4) &= \frac{1}{N_4} [\langle N_0^2 \rangle - \langle N_0 \rangle^2] \\ c_3(N_4) &= \frac{1}{N_4} [\langle N_0^3 \rangle - 3\langle N_0^2 \rangle \langle N_0 \rangle + 2\langle N_0 \rangle^3] \end{aligned} \quad (11)$$

The average is computed in the canonical ensemble. For a manifold with spherical topology and N_4 fixed, the number of nodes N_0 is linearly related to N_2 : $N_0 = N_2/2 - N_4 + 2$. Therefore the cumulants correspond to the second and the third derivative of the free energy with respect to κ_2 or, in other words, to the lattice version of the integrated 2- and 3-point connected correlators of the operator $\sqrt{g}R(x)$, where $R(x)$ denotes the scalar curvature. The two-point connected curvature–curvature correlator can be defined in an invariant manner, for example, as

$$c_2(r, V) = V^{-1} \left\langle \int d^4x \sqrt{g(x)} d^4y \sqrt{g(y)} \delta(r - |x - y|) [R(x)R(y) - \bar{R}^2] \right\rangle, \quad (12)$$

where $|x - y|$ is the geodesic distance between the points x and y , V is the (fixed) volume and $\bar{R} = V^{-1} \langle \int d^4x \sqrt{g(x)} R(x) \rangle$. We use here the more transparent continuum notation for convenience. Integrating $c_2(r, V)$ over r one gets the heat capacity $c_2(V) = V \{ \langle \bar{R}^2 \rangle - \langle \bar{R} \rangle^2 \}$. Notice that putting instead of the square bracket the expression $[R(x) - \bar{R}][R(y) - \bar{R}]$ one obtains a distinct correlator, but with the same integral. The non-uniqueness of the curvature-curvature correlator has already been noticed in [11]. For our purposes it is not necessary to settle this problem. We merely assume that there exists a definition compatible with the finite-size scaling of the integrated correlator.

In standard statistical mechanics the r -dependence of the two-point correlator in the neighbourhood of the continuous phase transition point is

$$c_2(r) \sim r^z C(|\kappa_2 - \kappa_2^*|^\nu r) \quad (13)$$

with $C(x)$ falling faster than a polynomial. The fall off of the correlator is controlled by the value of the mass gap $\sim |\kappa_2 - \kappa_2^*|^\nu$. The inverse of the mass gap, i.e. the correlation length, is the only relevant length scale. This has as a consequence the following finite-size scaling :

$$\begin{aligned} c_2(N_4) &= N_4^b f[(\kappa_2 - \kappa_2^*) N_4^c] \\ c_3(N_4) &= N_4^{b+c} f'[(\kappa_2 - \kappa_2^*) N_4^c] \end{aligned} \quad (14)$$

A pedestrian derivation of (14) consists in integrating both sides of (13) over a region of finite linear extension $\sim N_4^{\frac{1}{d_H}}$, d_H being the internal Hausdorff dimension of the system, at the critical point. One then gets (14) with $b = \alpha/d_H \nu$ and $c = 1/d_H \nu$, where $\alpha = \nu(1 + z)$ is to be identified with the specific heat exponent. Since $\alpha < 1$ for a continuous transition, one gets $b, c < 1$ using Fischer's hyperscaling relation $\alpha = 2 - d_H \nu$.

The equations (14) also hold when the transition is of first order. In this case one most easily obtain (14) using the fact that the distribution of the internal energy of the system has a bimodal shape in the neighborhood of the critical point. The finite-size scaling then reflects the existence of tunneling

between the two maxima. One easily finds that the exponents b and c are now strictly equal to unity: $b = c = 1$.

The function $f(x)$ in (14) is bell-shaped. Three values of its argument are of particular interest: they correspond to the maximum, zero and minimum of the derivative $f'(x)$. In what follows they are referred to by using the appropriate subscripts. Thus $f'(x_{max}) = \max[f'(x)]$, $f'(x_{min}) = \min[f'(x)]$, $f'(x_0) = 0$ and, of course, $f(x_0) = \max[f(x)]$.

We read the scaling of the maximum of the second cumulant with N_4 from the first of eqs. (14) :

$$\max [c_2(\kappa_2)] \sim N_4^b \quad (15)$$

the proportionality constant being equal to $f(x_0)$. The location of this maximum is $\kappa_2 = \kappa_{20}$ and is read from the equation $x = x_0$:

$$\kappa_{20} = \kappa_2^* + \frac{x_0}{N_4^c} \quad (16)$$

Analogously one finds

$$\begin{aligned} \max [c_3(\kappa_2)] &\sim N_4^{b+c} \\ \min [c_3(\kappa_2)] &\sim N_4^{b+c} \end{aligned} \quad (17)$$

The location of these structures is found from the right-hand side of eq. (16) after replacing x_0 by x_{max} and x_{min} , respectively.

The finite-size scaling functions in (14) do not include contributions to the cumulants originating from the non-singular terms in the free energy. This background must however be taken care of in the data analysis. Furthermore, the scaling sets in only at large enough volumes and, consequently, there are sub-leading corrections to the powers of volume appearing in the scaling formulae themselves. Thus analysing data taken at not too large N_4 one should, in general, replace N_4^c appearing in the argument of the scaling function by $N_4^c(1 + gN_4^\omega)$, say.

After all these preliminaries we are in a position to discuss the data produced in our numerical experiment (compare with [10, 8]). The second and the third cumulant, calculated for volumes ranging from $N_4 = 4000$ to 32000 are shown in Figs. 3 and 4, respectively, as functions of the coupling κ_2 . The curves and the error window have been obtained using reweighting [12]

together with the jack-knife method. The reweighting is a clever interpolation procedure, which combines in a non-trivial manner data obtained from runs with different coupling. This corresponds to an effective increase of the statistics and therefore the error window of the resulting curves tends to be smaller than the size of the errors of single measurements. However, reweighting is truly efficient when the set of couplings is sufficiently dense. Otherwise, although the procedure is doing its best to interpolate properly, the curve can occasionally miss some points. We have been more interested in the heights of peaks than in the exact shape of the curves. Therefore, we have decided to use our computer time to make precise measurements at these special points, where we had to fight against the critical slowing down, instead of making less precise measurements but on a dense grid of points.

Before entering the detailed quantitative discussion of these data, let us see what can be concluded from a rapid perusal of the figures. First of all, the curves corresponding to different volumes look very similar, modulo rescaling of the coordinate axes. Such a behavior is precisely what finite-size scaling predicts. One also notices that as one moves away from the critical point the cumulants come down to a higher value on the left than on the right-hand side. We shall see later that this asymmetry is to large extent due to a κ_2 -dependent background.

A more careful look at our figures indicates that the rate of growth of the structures increases with the volume. In particular, the change occurring as one moves from $N_4 = 16000$ to $N_4 = 32000$ is striking. As soon as we could contemplate the cumulant data at $N_4 = 32000$ we were led to suspect that a change of regime does occur in this last volume interval. Consequently we increased our statistics at $N_4 = 32000$ and close to the critical point, in order to see fine structures in the data. The result of this effort is shown in Fig. 5, where we display the energy (N_0) histogram with two clearly separated peaks, obtained at $N_4 = 32000$ and $\kappa_2 = 1.258$. The run history shows the system wandering between the two states. As one shifts κ_2 to 1.252 (or 1.264) the bimodality of the histogram stops being visible, at least with our statistics. However, the histogram is skew, compared to histograms observed at values of κ_2 more distant from the critical one or corresponding to smaller volumes. Furthermore, the run history shows that the system makes recurrent excursions to a neighbor state, where it does not stay for long, however.

Let us summarize what has been learned so far: all our data at $N_4 \leq$

16000 are compatible with the transition being continuous. But a double peak structure in the energy distribution is observed at $N_4 = 32000$. Such a bimodality developing with increasing volume is a signal of a first-order transition. The increase of the rate of growth of the structures in the critical region points in the same direction. In the rest of this section we show that the most natural description of all our data is obtained assuming that the exponents b and c are indeed equal to unity.

The estimated values of $\max[c_2]$ can be found in the last table of the Appendix. Assuming $\max[c_2]$ grows like in (15), i.e. as a power of the volume, one can calculate the exponent for successive pairs of neighbor volumes. One finds 0.30(5), 0.42(7) and 0.81(9) for the first, second and third pair of points. Thus the effective exponent increases with the volume. When a fit to all points is attempted with the power law (15) the exponent is $b = 0.41(2)$. However the fit is bad, $\chi^2/dof = 23.5$, and it misses the point at $N_4 = 32000$.

A considerably better description is obtained from a linear fit, assuming a nonvanishing background. Assuming that $\max[c_2]$ is linear in both N_4 and κ_{2max} we obtain the fit $\max[c_2] = 0.80(7) \times 10^{-5}N_4 + 0.267(94) - 0.161(90)\kappa_{2max}$, with $\chi^2/dof = 4.6$. The background, which corresponds to the second and third term in this fit, is shown as a dotted straight line in Fig. 3. Notice that a background decreasing with κ_2 fits well with the observed structure of the histogram in Fig. 5, where the left peak, corresponding to the lower κ_2 phase, is wider than the right one.

Consider now the third cumulant. A quantity of particular interest is $\max[c_3] - \min[c_3]$, since it is independent of the κ_2 -independent part of the background. We fit its N_4 -dependence with a fixed power and with a parabola. In the former case we get an exponent 1.79(14) close to the first-order transition exponent 2 ($\chi^2/dof = 10.0$). Assuming that the exponent is 2 but introducing next-to-leading corrections we fit better the data with the parabola $0.30(4) \times 10^{-7}N_4^2 - 0.17(9) \times 10^{-3}N_4 + 0.9(3)$ ($\chi^2/dof = 5.5$).

The last part of the data analysis concerns the positions of the characteristic points of the scaling function $f(x)$. We first try the formula (compare with (16))

$$\kappa_{2j}(N_4) = \kappa_2^* + \frac{x_j}{N_4^c} \quad (18)$$

with $j = \{max, 0, min\}$ to fit 12 data points corresponding to four volumes and three positions: maximum, zero and minimum of the third cumulant.

In the functions $\kappa_{2j}(N_4)$ we keep the values of κ_2^* and c common, so that the three curves only differ by the numerator x_j of the second term. Hence, altogether we have 12 data points and five free parameters. We obtain $c = 0.47(7)$, $\kappa_2^* = 1.327(13)$ and $\chi^2/dof = 24.5$.

An alternative fit, more appropriate for a first-order transition, is obtained using the formula

$$\kappa_{2j}(N_4) = \kappa_2^* + \frac{x_j}{N_4 + a_4} \quad (19)$$

The number of free parameters is the same as before. We get now $\kappa_2^* = 1.293(4)$, $a_4 = 5234(1018)$ and $\chi^2/dof = 8.3$. The other parameters are $x_{min} = -1.54(17) \times 10^3$, $x_0 = -1.39(17) \times 10^3$, $x_{max} = -1.16(15) \times 10^3$. The fit is illustrated in Fig. 6, where $\kappa_{2j}(N_4)$ should be read on the vertical axis and $1000/(N_4 + 5234)$ on the horizontal one.

Our conclusions rest heavily on results obtained at $N_4 = 32000$ and are sensitive to data taken at small N_4 . Therefore, it will be very important to extend this study to larger lattices. Until this is done our conclusions will remain somewhat tentative. Extrapolating the last fit we expect that the bimodality of the N_0 histogram will show up at in the neighborhood of $\kappa_2 = 1.267$ for $N_4 = 48000$ and at $\kappa_2 = 1.273$ for $N_4 = 64000$ ⁶.

5. Discussion

The most important new result of this paper is the evidence that the phase transition of the model is of first order. We have started this study persuaded, as everybody, that in $4d$ the transition is continuous. The surprising discovery of signals of a discontinuous transition requires a reevaluation of the standard picture. Therefore it is important to formulate a number of caveats.

One can, of course, extend the study to larger systems in order to check the expectations formulated in the preceding section. Most likely these expectations will be confirmed if a standard simulation set-up is used. One

⁶While completing our manuscript we have submitted a job with $N_4 = 48000$, $\kappa_2 = 1.267$. A flip between the phases occurs after roughly 20000 sweeps. B.V. de Bakker and J. Smit being informed about our predictions have looked at their data files in search for the expected double peak structure and have indeed found a time history flipping between two states for $N_4 = 64000$ near the expected value of κ_2 .

can wonder, however, whether or not the discontinuous phase transition is an artifact of the algorithm employed. The latent heat of the transition is quite small (e.g. in comparison with $3d$, where a first order transition has been observed). The moves employed in the simulation are not suspect by themselves. However, the constraint limiting volume fluctuations might not be innocuous ⁷. Strictly speaking, the proof of ergodicity does hold when there is no limitation imposed on multiplicity of simplexes in intermediate configurations. It might be that there exists a set of paths requiring large departures from the volume where the measures are performed and connecting the two states we observe at the transition point. Then, by excluding these paths one would create artificially a "potential barrier". We have checked that our results are not affected when one changes the parameter δ , multiplying the quadratic term in the action, by an order of magnitude (from 0.005 to 0.0005). Further investigation in this direction would be important and desirable.

Our renormalization group study confirms and strengthens the results presented in ref. [2]. There is a value of κ_2 , close to the transition point found by other methods, where the manifolds appear to show a self-similar structure under the RG transformation. In the neighbourhood of this point the intrinsic Hausdorff dimension, measured along the RG flow, is close to $d_H = 4$ instead of being 2 or ∞ . Thus, from these data alone one would claim that the model has an isolated ultra-violet stable fixed point and that one can define a sensible continuum limit letting $\kappa_2 \rightarrow \kappa_2^*$, $N_4 \rightarrow \infty$ in a way insuring that the lattice spacing a tends to zero when measured in physical units ⁸. The RG analysis has been performed for volumes up to $N_4 = 16000$ while the bimodal distribution of N_0 is only observed at $N_4 = 32000$. If the first-order phase transition signal is an algorithm artifact and if the algorithm becomes unreliable only at volumes larger than $N_4 = 16000$ then our RG results may still retain their full significance.

If the transition is not an artifact then the relevance of our RG study is

⁷This has been already mentioned by other people, in particular in ref. [13], where an attempt has been made to check the point at $\kappa_2 = 0$. No signal of a breakdown of ergodicity was found, but the accepted deviations from the reference volume were still modest.

⁸This limit would presumably preserve the global geometry of manifolds, in particular the fractal dimension d_H . The existence of the graviton is a separate issue. Notice that in $2d$, where the graviton is absent, one can nevertheless define a continuum limit.

uncertain. This failure of the RG method to show a discontinuous transition could be attributed to either an inadequacy of the blocking method or to the presence of finite size effects which, as we have discussed, cannot be eliminated in the present formulation.

It should be stressed that our RG results are based on the volume-volume correlations only. The corresponding characteristic length scale is $\langle r \rangle$. To further understand the dynamics of the model it is necessary to study also the curvature-curvature correlations, which are controlled by another length scale, essentially the inverse mass of the lattice "graviton". This has been the motivation of our finite-size scaling analysis of the moments of the node distribution.

It is not surprising to have a finite mass gap on the lattice, i.e. as long as one does not take the continuum limit. Indeed, the discrete theory is not endowed with the continuous gauge symmetry implying the existence of the graviton. But it is natural to expect that this mass gap scales to zero as one approaches the critical point, so that in the continuum limit one has a chance of recovering a massless graviton. But this means that the transition is continuous. If this reasoning is correct and if the discontinuity of the phase transition is an intrinsic feature of the model than the latter is not an acceptable model of quantum gravity.⁹

It is clear that the surprising discovery presented in this paper raises a series of questions. Let us hope that they will be rapidly resolved by a joint effort of all groups interested in the development of lattice gravity.

Acknowledgements

We thank B.V. de Bakker, J. Jurkiewicz and J. Smit for conversations. We are indebted to J. Jurkiewicz for providing us the opportunity to check our code against his. We are grateful to B. Klosowicz for very precious help. We are indebted to the CNRS computing center IDRIS, and personally to V. Alessandrini, for computer time and cooperation. We are also indebted

⁹It has been pointed out to us by J. Smit that the continuity of the transition is perhaps not necessary: There exist models with a Coulomb phase and no continuous transition. In the $Z(N)$ gauge model studied in ref. [14] the Coulomb phase appears at finite N . Due to quantum tunneling the model anticipates the $U(1)$ symmetry which becomes manifest in the action in the limit $N \rightarrow \infty$ only.

to IC3A for computer time on POWERXPLORER at SARA and the HLRZ Jülich for computer time on PARAGON. P.B. thanks the Stichting voor Fundamenteel Onderzoek der Materie (FOM) for financial support. Z.B. has benefited from the financial support of the Deutsche Forschungsgemeinschaft under the contract Pe 340/3-3.

References

- [1] D. Weingarten, Nucl. Phys. B210 [FS6] (1982) 229; F. David, Nucl. Phys. B257 (1985) 543; J. Ambjørn, B. Durhuus and J. Fröhlich, Nucl. Phys. B257 (1985) 433; V.A. Kazakov, I.K. Kostov and A.A. Migdal, Phys. Lett. B157 (1985) 295.
- [2] Z. Burda, J.-P. Kownacki and A. Krzywicki, Phys. Lett. B356 (1995) 466.
- [3] S. Bilke, Z. Burda and J. Jurkiewicz, Comp. Phys.Comm. 85 (1995) 278.
- [4] J. Ambjørn, P. Bialas, Z. Burda, J. Jurkiewicz and B. Petersson, Phys. Lett. B325 (1995) 337.
- [5] J. Ambjørn and J. Jurkiewicz, Nucl. Phys. B451 (1995) 643.
- [6] S. Catterall and G. Thorleifsson, Syracuse preprint SU-4240-619, hep-lat/950003, to be published in Nucl. Phys. B.
- [7] B.V. de Bakker and J. Smit, Nucl. Phys. B439 (1995) 239.
- [8] S. Catterall, J. Kogut and R. Renken, Phys. Lett B328 (1994) 277.
- [9] J. Ambjorn, Z. Burda, J. Jurkiewicz and C.F. Kristjansen, Acta Phys. Pol. 23B (1992) 991.
- [10] J. Ambjørn and J. Jurkiewicz, Phys. Lett. B278 (1992) 42.
- [11] B.V. de Bakker and J. Smit, Nucl. Phys B454 (1995) 343.
- [12] M. Falconi, E. Marinari, M.L. Paciello, G. Parisi and B. Taglienti, Phys. Lett. 108B (1982) 331; E. Marinari, Nucl. Phys. B235 (1984) 123 ; G. Bhanot, S. Black, P. Carter and R. Salvador, Phys. Lett. 183B (1986) 331; 63 (1989) 1195. A.M. Ferrenberg and R.H. Swendsen, Phys. Rev. Lett. 61 (1988) 2635; 63 (1989) 1195.
- [13] S. Catterall, G. Thorleifsson, J. Kogut and R. Renken, *Singular Vertices and the Triangulation Space of the D-sphere*, Syracuse preprint hep-lat/9512012.

- [14] V. Alessandrini, Nucl. Phys. B215 (1983) 337; V. Alessandrini and Ph. Boucaud, Nucl. Phys. B225 (1983) 303.

Figure captions

- Fig. 1** - The integral τ of the autocorrelation function (in sweeps) versus κ_2 for different volumes. The symbols corresponding to different volumes are 4000(+), 8000(\times), 16000(\times) and 32000(\square). The quantity measured is N_0 . The τ 's for other observables are comparable, with the exception of N_{4out} , for which τ is never larger than 100 sweeps.
- Fig. 2** - The nonperturbative β -function for $N_4 = 4000(\times)$, 8000(\times) and 16000(\square). The zeros are at $\kappa_2 = 1.178(10)$, 1.217(4) and 1.240(2), respectively.
- Fig. 3** - The second cumulant c_2 as a function of κ_2 for lattice size $N_4 = 4000(+)$, 8000(\times), 16000(\times) and 32000(\square). The distance between the upper and lower lines gives the error window. The dotted line is a background fitted to the linear form as discussed in the text.
- Fig. 4** - The third cumulant c_3 as a function of κ_2 for lattice size $N_4 = 8000(+)$, 16000(\times) and 32000(\times). The distance between the upper and lower lines gives the error window.
- Fig. 5** - The histogram for N_0 at $N_4 = 32000$ and $\kappa_2 = 1.258$. The number of 7×10^4 entries gathered every 50th sweep comes from 3.5×10^6 sweeps corresponding to 508 integrated autocorrelation times. The solid line is obtained by averaging over bins of N_0 of length 20.
- Fig. 6** - The position of the maxima zeros and minima of the third cumulant versus $1000/(N_4 + 5234)$. The dashed lines are obtained fitting $\kappa_2^* + x/(N_4 + a_4)$ to all those 12 points, in such a way that all three lines have a common value of κ_2^* and a_4 but different values of x .

Appendix

	$N_4 = 4000$			$N_4 = 3000$
κ_2	$\langle r_{in} \rangle$	$\langle r_{out} \rangle$	$\langle N_{4out} \rangle$	$\langle r_{in} \rangle$
1.025	11.93(6)	11.03(5)	3370(10)	-
1.050	12.38(6)	11.34(5)	3304(10)	12.09(8)
1.075	12.79(11)	11.65(11)	3245(15)	12.58(8)
1.100	13.59(26)	12.28(23)	3163(13)	13.36(30)
1.125	15.33(44)	13.88(41)	3094(10)	15.11(46)
1.150	16.37(62)	14.83(61)	3044(11)	16.26(32)
1.175	19.42(44)	17.67(43)	2965(8)	17.52(31)
1.200	20.97(40)	19.20(40)	2934(6)	18.72(28)
1.225	21.73(21)	19.87(21)	2910(7)	19.35(21)
1.250	23.10(17)	21.19(17)	2878(5)	-

Table 1: RG study: data for $N_4 = 4000$

	$N_4 = 8000$			$N_4 = 6000$
κ_2	$\langle r_{in} \rangle$	$\langle r_{out} \rangle$	$\langle N_{4out} \rangle$	$\langle r_{in} \rangle$
1.100	14.03(9)	12.85(5)	6491(22)	-
1.125	14.81(11)	13.48(11)	6327(12)	14.79(10)
1.150	15.86(17)	14.37(17)	6193(10)	16.47(34)
1.175	17.75(38)	16.11(37)	6055(10)	18.86(40)
1.200	23.03(49)	21.22(48)	5918(13)	23.19(30)
1.225	27.86(39)	25.94(38)	5834(7)	25.63(28)
1.250	30.45(22)	28.44(21)	5783(9)	27.44(22)
1.275	32.12(34)	30.05(34)	5753(9)	28.10(16)
1.300	33.96(23)	31.83(22)	5684(6)	29.61(15)
1.325	34.46(23)	32.33(22)	5672(6)	-

Table 2: RG study: data for $N_4 = 8000$. The errors on N_{4out} are much smaller than those given in ref. 1. This is partly due to the use of a more efficient algorithm and partly to the elimination of a bug.

	$N_4 = 16000$			$N_4 = 12000$
κ_2	$\langle r_{in} \rangle$	$\langle r_{out} \rangle$	$\langle N_{4out} \rangle$	$\langle r_{in} \rangle$
1.125	15.42(4)	14.22(4)	12898(14)	-
1.150	16.20(5)	14.82(4)	12585(12)	16.20(11)
1.175	17.45(11)	15.90(11)	12284(12)	17.19(8)
1.200	19.08(16)	17.38(15)	12045(8)	21.04(46)
1.213	20.85(35)	19.06(34)	11901(12)	24.92(88)
1.225	25.92(48)	24.01(47)	11768(6)	28.31(92)
1.238	34.58(70)	32.56(70)	11655(5)	33.18(57)
1.250	38.22(76)	36.12(76)	11586(4)	35.64(39)
1.262	42.13(42)	40.02(42)	11529(7)	37.62(29)
1.275	43.59(38)	41.41(37)	11488(4)	38.62(27)
1.300	46.01(17)	43.79(17)	11412(5)	40.63(20)
1.325	47.88(22)	45.61(22)	11356(5)	-

Table 3: RG study: data for $N_4 = 16000$

κ_2	c_1	c_2	c_3	τ	#sweeps	# τ 's
1.075	0.17089(20)	0.097(3)	0.07(8)	194(26)	247480	1276
1.100	0.17598(16)	0.106(3)	0.05(6)	256(27)	562090	2196
1.125	0.18172(17)	0.111(3)	0.14(5)	344(38)	674730	1961
1.137	0.18401(17)	0.113(2)	-0.01(5)	434(46)	905340	2086
1.150	0.18738(23)	0.109(3)	-0.36(9)	419(60)	436380	1042
1.175	0.19261(16)	0.085(3)	-0.48(7)	264(31)	438020	1659
1.200	0.19680(22)	0.064(4)	-0.39(11)	239(42)	163840	685
1.225	0.19891(22)	0.060(4)	-0.26(7)	135(24)	89180	661
1.250	0.20170(10)	0.049(1)	-0.16(2)	69(7)	163840	2374

Table 4: Cumulants: data summary for $N_4 = 4000$. We denote by c_1 , c_2 and c_3 the first three cumulants of the N_0 distribution, normalized to the volume N_4 ($c_1 = \langle N_0 \rangle / N_4$). The parameter τ is the integrated autocorrelation time. In the last two columns we put the number of sweeps performed and an estimate of the number of autocorrelation times to which this number of sweeps corresponds.

κ_2	c_1	c_2	c_3	τ	#sweeps	# τ 's
1.100	0.16853(16)	0.097(3)	0.15(15)	167(24)	163840	981
1.125	0.17332(20)	0.101(4)	-0.01(15)	247(45)	163840	663
1.150	0.17926(16)	0.124(4)	0.24(13)	451(60)	572750	1270
1.163	0.18237(16)	0.117(4)	0.12(13)	422(58)	491520	1165
1.175	0.18507(19)	0.137(6)	0.51(19)	721(109)	667180	925
1.187	0.18859(17)	0.143(4)	0.03(12)	846(113)	1055340	1247
1.190	0.18929(22)	0.149(5)	-0.52(19)	939(139)	694160	739
1.200	0.19233(20)	0.120(4)	-0.84(15)	839(137)	645820	770
1.225	0.19762(15)	0.069(4)	-0.55(14)	209(35)	163840	783
1.250	0.20054(7)	0.054(2)	-0.26(4)	152(14)	458750	3018
1.300	0.20510(6)	0.039(1)	-0.10(3)	52(5)	163840	3150

Table 5: Cumulants: data summary for $N_4 = 8000$. The notation is the same as for the table for $N_4 = 4000$.

κ_2	c_1	c_2	c_3	τ	#sweeps	# τ 's
1.125	0.16749(21)	0.110(9)	0.19(38)	233(59)	81920	352
1.150	0.17317(20)	0.104(6)	-0.18(29)	229(57)	81920	358
1.175	0.17914(30)	0.130(9)	0.13(48)	433(140)	81920	189
1.200	0.18462(9)	0.132(5)	1.05(34)	647(72)	1262800	1952
1.213	0.18813(10)	0.133(4)	0.64(29)	726(89)	1136040	1565
1.225	0.19228(18)	0.190(7)	1.10(38)	2022(332)	1551360	767
1.228	0.19388(23)	0.198(6)	-1.17(61)	2342(476)	1396500	596
1.238	0.19669(15)	0.144(6)	-3.27(33)	1735(274)	1419640	818
1.250	0.19928(16)	0.083(4)	-0.86(17)	596(137)	245760	412
1.262	0.20113(13)	0.054(4)	-0.59(21)	174(39)	81920	471
1.275	0.20241(7)	0.049(3)	-0.28(13)	108(15)	163840	1517
1.300	0.20454(5)	0.040(1)	-0.12(6)	50(5)	163840	3276
1.325	0.20644(5)	0.037(1)	-0.09(5)	36(4)	122880	3413

Table 6: Cumulants: data summary for $N_4 = 16000$. The notation is the same as for the table for $N_4 = 4000$.

κ_2	c_1	c_2	c_3	τ	#sweeps	# τ 's
1.240	0.18970(12)	0.141(7)	0.58(58)	1046(188)	674900	645
1.246	0.19150(11)	0.144(8)	0.96(67)	1124(194)	786950	700
1.252	0.19399(32)	0.254(35)	12.21(220)	6419(2183)	1000350	156
1.258	0.19712(20)	0.316(8)	-6.10(205)	6883(1352)	3502350	508
1.264	0.20052(21)	0.118(20)	-9.05(353)	4064(1326)	695650	171
1.270	0.20085(27)	0.118(20)	-6.56(163)	3027(1269)	304850	101

Table 7: Cumulants: data summary for $N_4 = 32000$. The notation is the same as for the table for $N_4 = 4000$.

N_4	c_{2max}	c_{3max}	c_{3min}	κ_{2max}	κ_{3max}	κ_{3min}
4K	0.116(1)	0.18(5)	-0.53(3)	1.1380(25)	1.1145(41)	1.1747(22)
8K	0.143(3)	0.54(9)	-1.21(9)	1.1886(12)	1.1756(17)	1.2085(14)
16K	0.191(5)	1.94(22)	-3.35(24)	1.2267(8)	1.2189(9)	1.2368(8)
32K	0.335(13)	13.2(13)	-17.0(14)	1.2565(4)	1.2528(4)	1.2606(4)

Table 8: The heights and positions of the maximum of the second cumulant and of the maximum and minimum of the third one for different volumes.

FIGURE 1

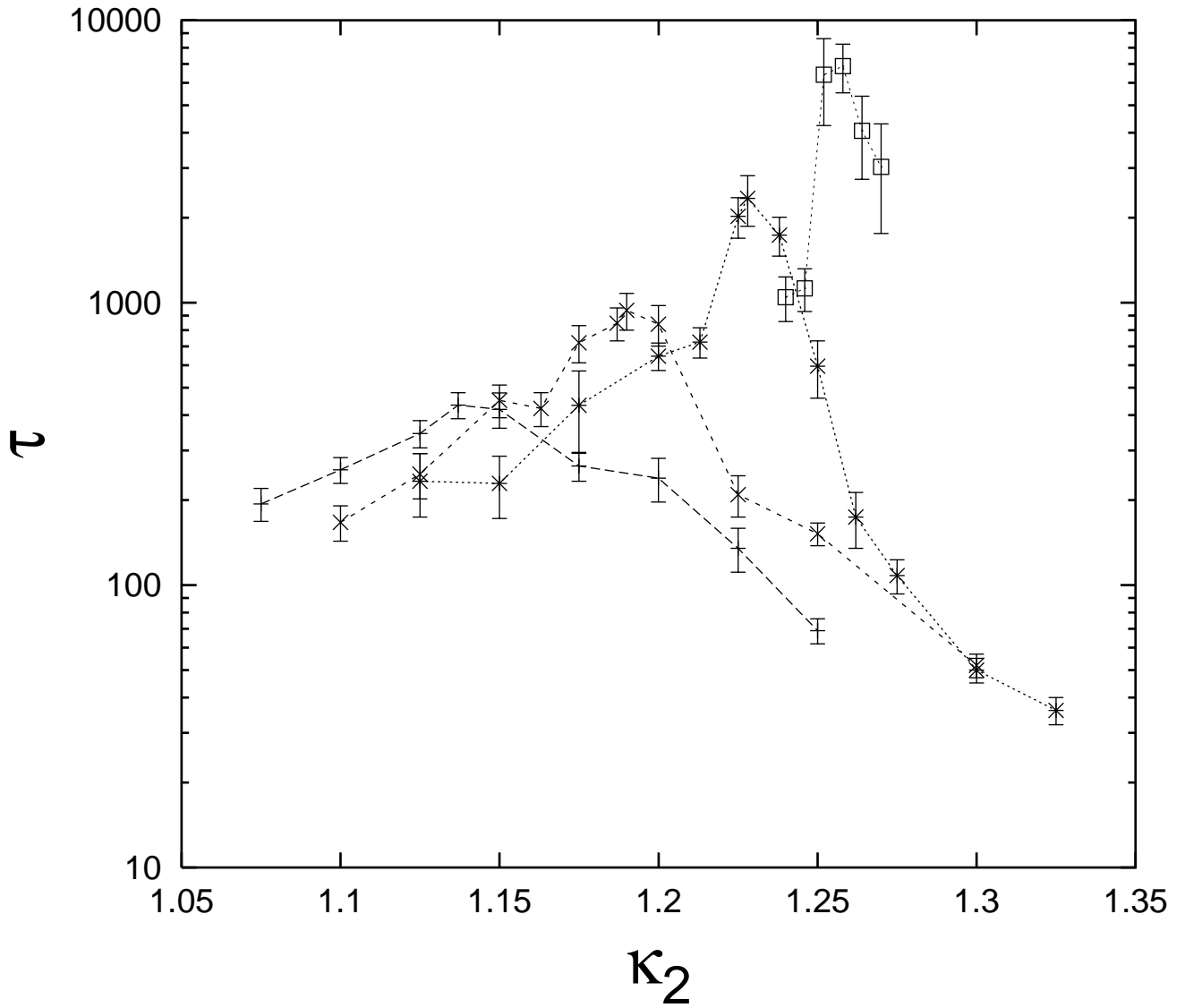


FIGURE 2

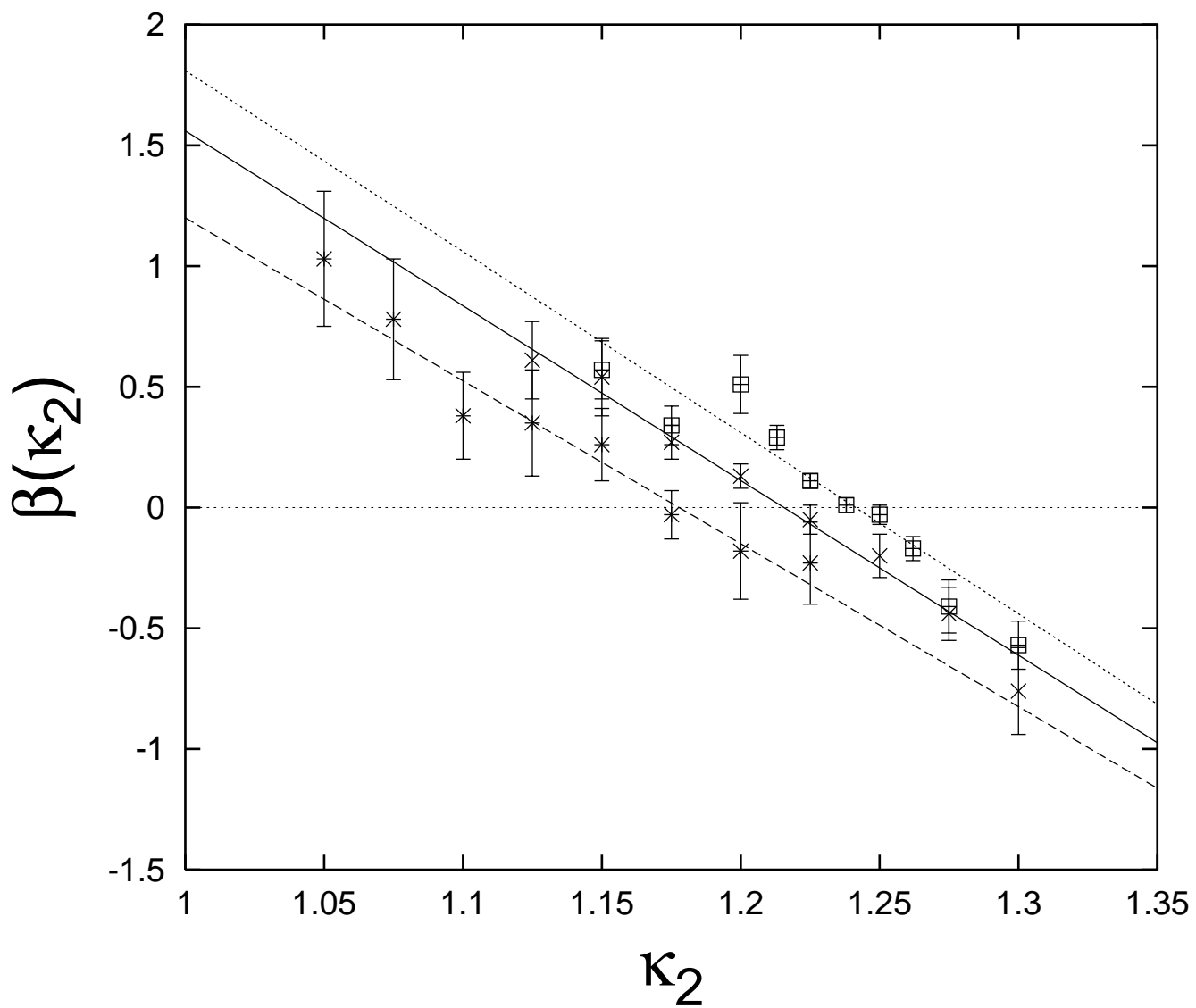


FIGURE 3

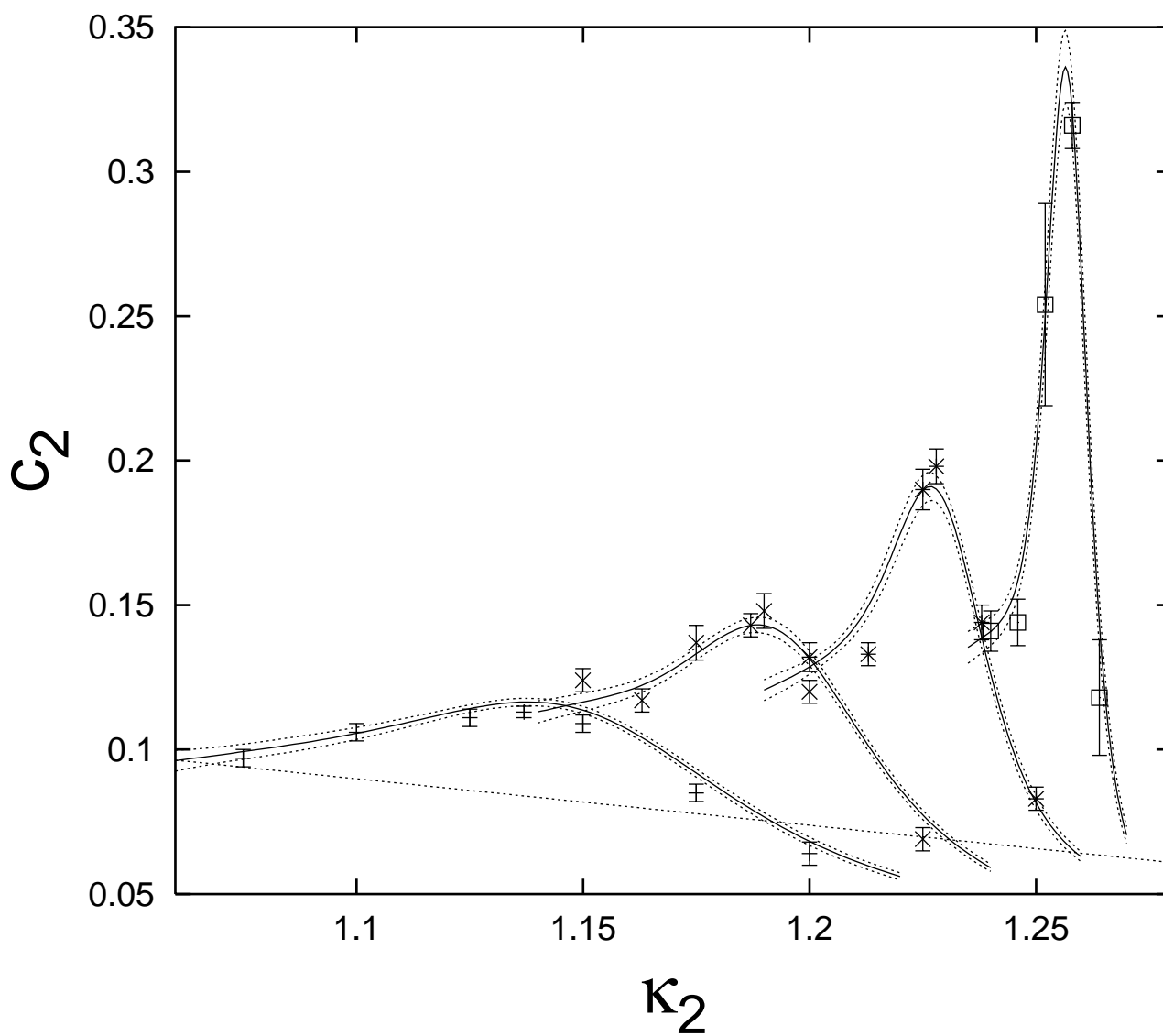


FIGURE 4

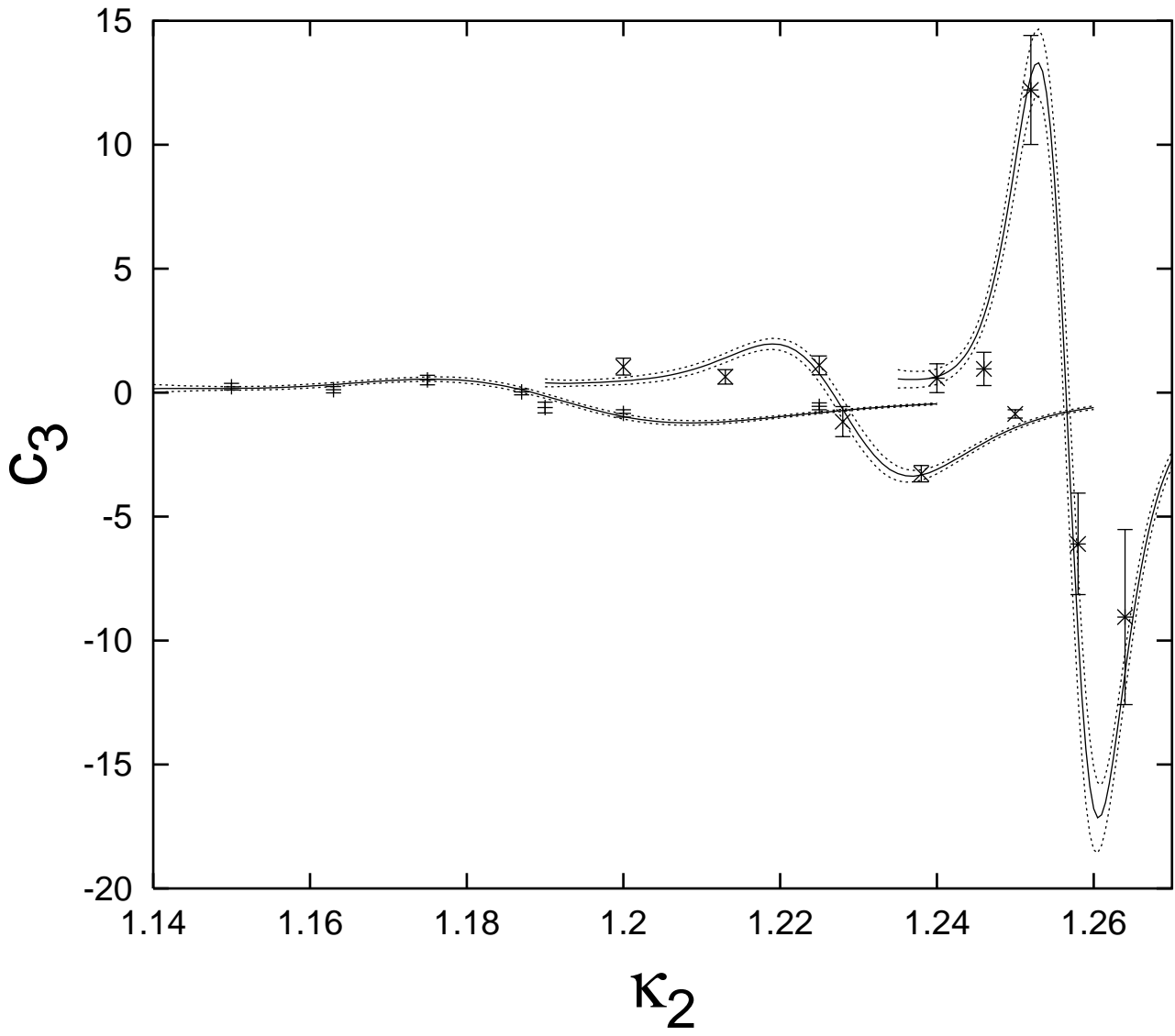


FIGURE 5

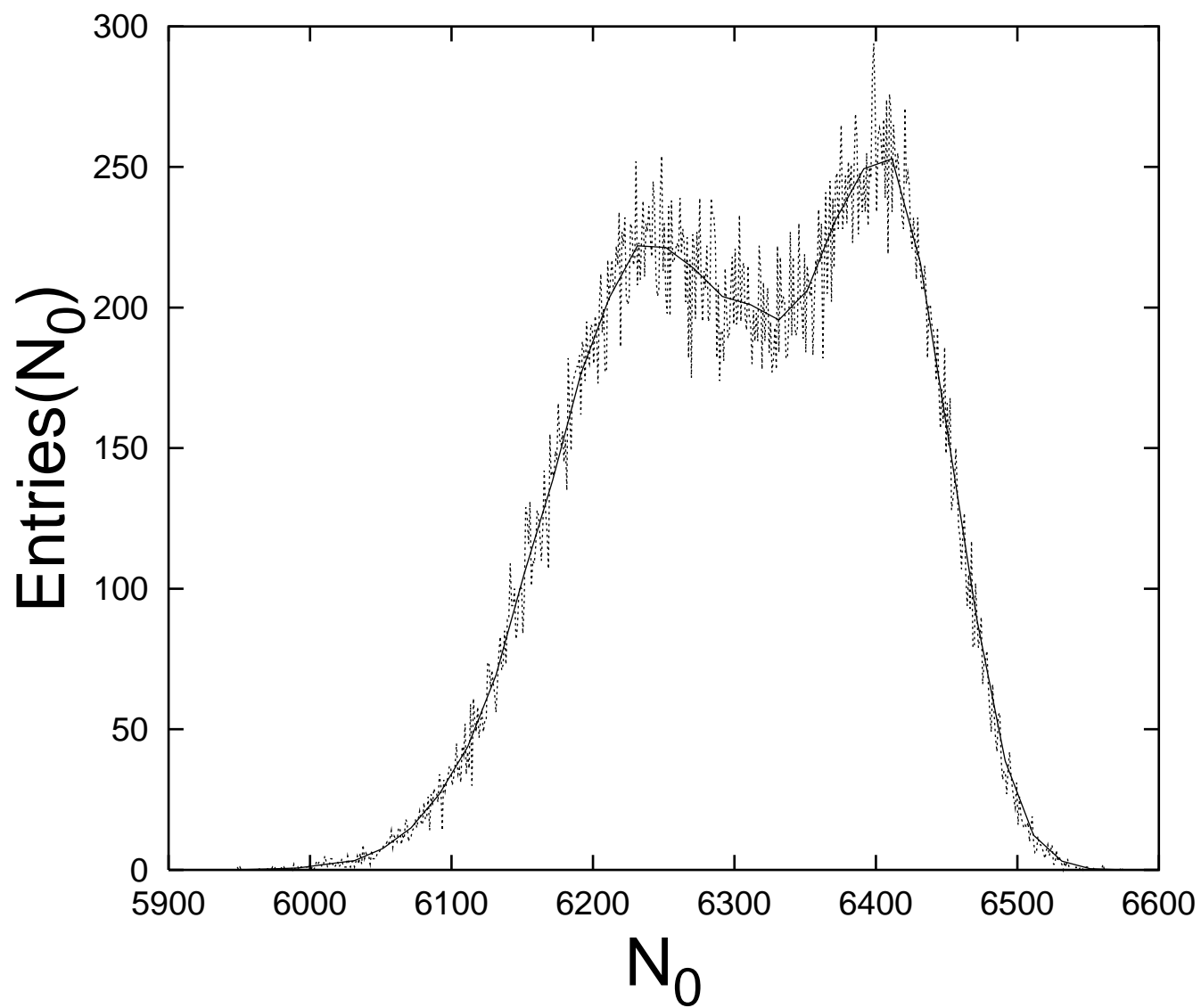


FIGURE 6

